Electronic Supplementary Material (ESI) for Lab on a Chip.

Supplementary Information

Beating heart on a chip: a novel microfluidic platform to generate functional 3D cardiac microtissues

Authors: Anna Marsano[1], Chiara Conficconi[1,2]*, Marta Lemme[1,2]*, Paola Occhetta[2], Emanuele Gaudiello[1], Emiliano Votta[2], Giulia Cerino[1], Alberto Redaelli[2], and Marco Rasponi[2]

Affiliations

[1] Departments of Surgery and Biomedicine, University Basel, University Hospital Basel, Basel, Switzerland

[2] Department of Electronics, Information and Bioengineering, Politecnico di Milano, Milano, Italy

* These authors equally contributed to this work

Corresponding authors

Marco Rasponi
Piazza Leonardo da Vinci 32
Building #21
20133 Milano, Italy.
Tel.: +39 02 2399 3377
Fax: +39 02 2399 3360
Email: marco.rasponi@polimi.it

Anna Marsano
Cardiac Surgery and Engineering Group
Department of Biomedicine, Hebelstrasse 20
4031 Basel, Switzerland
Tel.: +41 061 32 87448
Fax.: +41 061 265 3990
Email: anna.marsano@usb.ch

Electric field calculation

In general, the electric field acting on cells in culture is approximated by dividing the applied voltage by the distance between electrodes. Although this is strictly valid only in the case of two parallel electrodes within a container featuring parallel faces, it still remains a good approximation in most macroscale setups. However, this condition does not apply to the present device, which is characterized by a microscale and rather complex geometry. Thus, a numerical model was developed to quantify the electric field acting on the micro-cardiac constructs.

A commercial FEM software package (Comsol Multiphysics) was used to generate a geometrical model resembling the cell culture compartment, and subsequently discretize it through a tetrahedral mesh scheme consisting of about 610,000 elements. At the boundaries, constant voltage conditions were applied in correspondence to the regions occupied by electrodes (1V and 0V, respectively), while electrical insulation was applied to the remaining outer walls. The electric field was calculated by solving Maxwell's equations with the electroquasistatic approximation, using a conductivity of 1.5 S/m(36).

The electric field expected by dividing the voltage applied (1V) by the distance between electrodes (about 16mm) is constantly equal to 0.625 V/cm. Fig. S7 shows the top view distribution of the electric field within the device calculated with the numerical model. When considering only the region occupied by the cell-laden gel, the electric field vector is mainly aligned to the main axis of the micro-engineered cardiac construct, as evidenced by the preponderance of the parallel component (E_y, top), with respect to the orthogonal (E_x, bottom) and the vertical (E_z, not shown in the figure) ones. In particular, by neglecting the border effect, the intensity of the electric field E in the gel region is almost constant and equal to 0.121 V/cm. The electric potential across the construct length drops of about 0.11V, which represents the effective electric potential drop perceived by cells.

Indeed, most electric field is dissipated within the small auxiliary channels, which are thinner and shorter than the culture compartment. As represented in the Fig. S7, fluidic channels behave as

electrical resistors, proportional to their lengths and inversely proportional to their cross-sectional areas. An electric equivalent circuit could be implemented, eliciting from geometrical considerations. The electric potential drop across the cells in culture was estimated through a voltage divider given by $R_2/(R_1+2R_2)$. The resulting factor, equal to 1/8.2 (≈ 0.122), was applied to correct the external electric field during experiments thus providing the actual electric potential perceived by cells.

Supplementary Figures

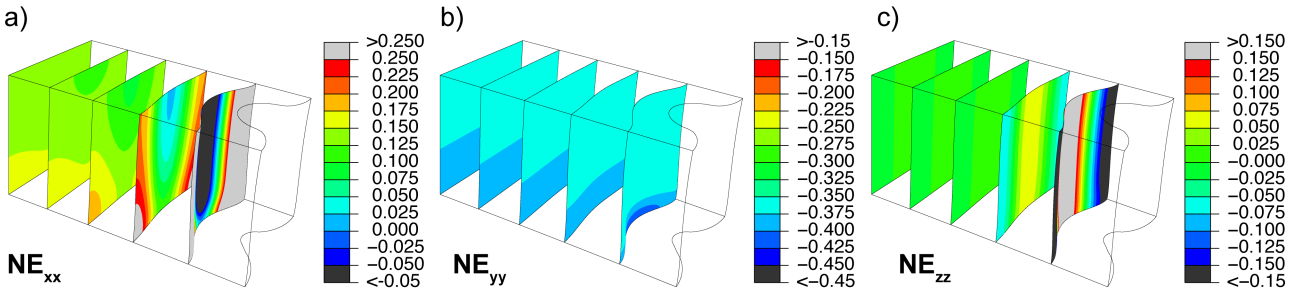

Fig. S1. Finite element computation of the spatial distribution of gel normal nominal strains in the pillar-to-pillar direction (NE_{xx}, panel a), in the vertical direction (NE_{yy}, panel b), and along the axis of the microfluidic channel (NE_{zz}, panel c). For each strain component, results are depicted at five sections throughout the gel dimension in the pillar-to-pillar dimension. Sections correspond to planes located at 0, 30, 60, 90, and 120 μm from the symmetry plane of the microfluidic channel at when the device is in its undeformed condition.

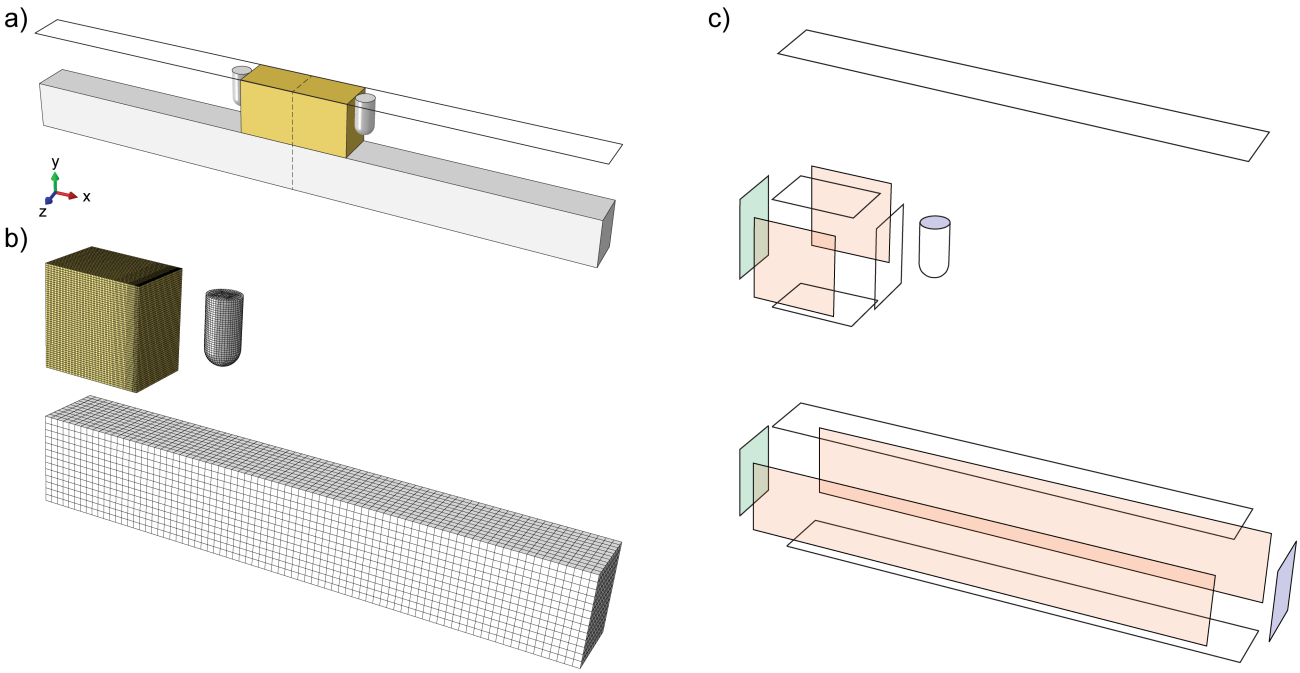

Fig. S2. Geometrical model for the FEM analysis. (a) Repetitive unit of the microfluidic channel in its unloaded configuration. The key elements of the repetitive unit are depicted: PDMS membrane and PDMS pillars (light grey), channel ceiling (transparent), and gel (bronze). (b) Discretized geometry of half of the gel bulk, half of the PDMS membrane and one PDMS pillar, which compose half of the repetitive unit, as actually considered in the finite element model. (c) Representation of the model regions constrained through boundary conditions: violet surfaces (i.e. upper end of the PDMS pillar and right hand end of the PDMS membrane) were prevented from any rigid motion; light green surfaces were prevented from translations along the x-direction and rotations along the y- and z-direction, owing to the symmetry of the repetitive unit; light red surfaces were prevented from translations along the z-direction and rotations along the x- and y-direction, owing to the periodicity of the system along the z-direction.

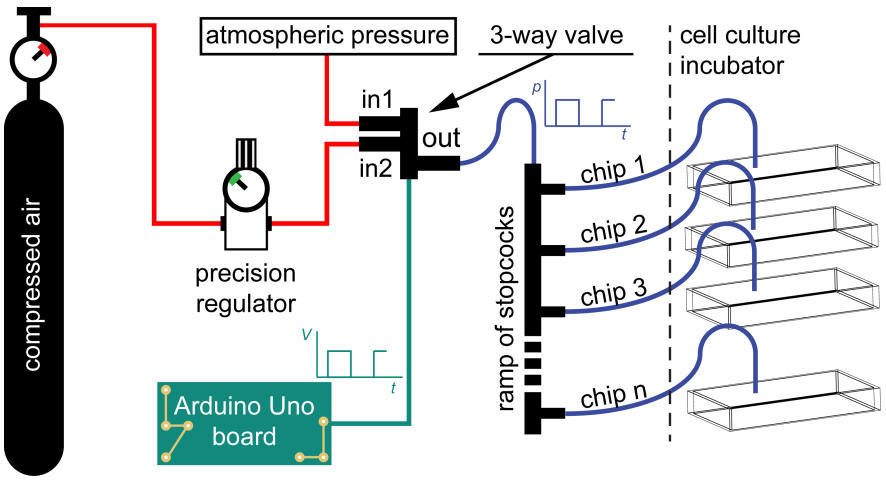

Fig. S3. Electro-pneumatic control system. An electro-pneumatic control system was assembled to perform the cyclic mechanical stimulation. A compressed air cylinder was used as a pressure source, while the pressure level was controlled and maintained constant through a precision regulator. A three-way miniature valve was used to transmit to its output either the controlled pressure line or the atmospheric pressure. A ramp of stopcocks was connected to the miniature valve outlet to multiply the number of addressable microfluidic devices. Switching between input pressure values was achieved through a custom-made electronic controller based on the Arduino Uno microcontroller board. The stimulation frequency, easily tunable according to the specific experimental design, was set equal to 1Hz.

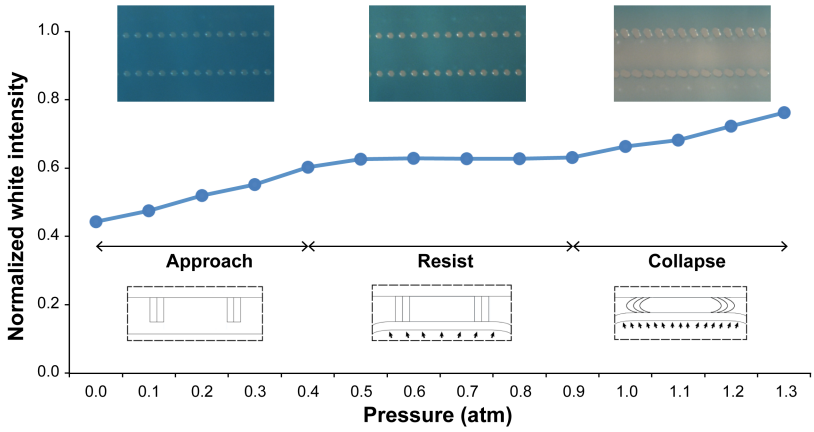

Fig. S4. Microdevice mechanical characterization: curve pressure-compression. A preliminary mechanical characterization of microdevices (N=16) was performed to find a correlation between the pressure applied in the actuation chamber and the membrane displacement. The microfluidic chamber was filled with a blue dye solution that, when no pressure was applied, completely occupied the gap between micro-posts and membrane: in this condition micro-posts bottom surfaces appeared blue colored. The pressure was gradually increased (from 0atm to 1.3atm, steps=0.1atm) and the normalized white intensity of the micro-posts bottom surfaces was used as an estimator of membrane displacement. By increasing the pressure level up to 0.4atm, the resulting displacement of the membrane towards the micro-posts caused a gradual whitening of their surface ("approach" phase). When the contact was reached, the gap was not filled anymore by the blue dye solution, and the micro-posts bottom surfaces appeared white ("resist" phase). In this condition (pressure ranging between 0.5atm and 0.9atm) the normalized white intensity stabilized around an asymptotic value. Further increases in the applied pressure caused the collapse of the micro-posts, which started to bend causing the white intensity value to diverge from the plateau ("collapse" phase).

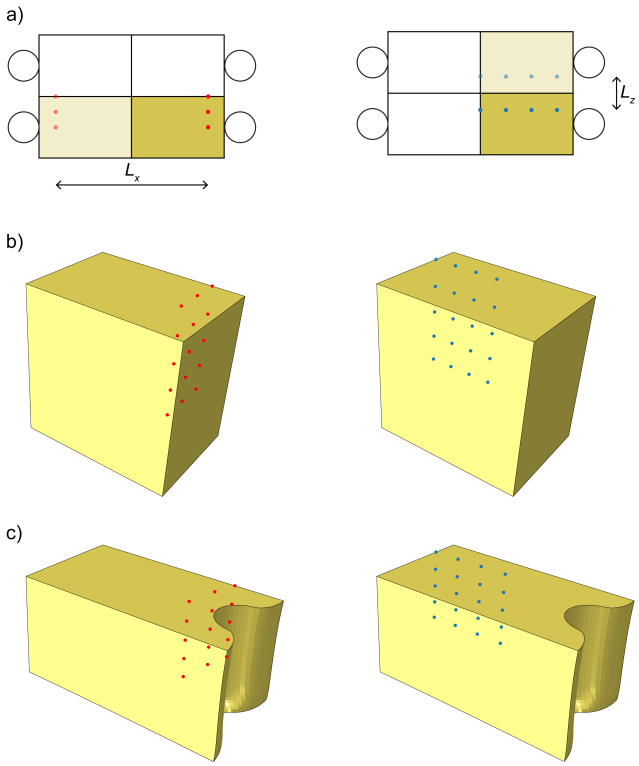

Fig. S5. Mimicking experimental strain measurement on the FEM. (a) Measurement of nominal strains on the finite element model, mimicking the experimental measurement for comparison purposes. Strains in the pillar-to-pillar direction (NE_{xx}) and along the axis of the microfluidic channel (NE_{zz}) were obtained selecting nodes on the finite element model (dots in the dark yellow region) consistently with the criteria adopted in the experimental measurements, and computing the changes in distances L_x and L_z, respectively, between the selected points and those obtained by mirroring them with respect to the symmetry plane (NE_{xx}, red dots) and the periodic boundary (NE_{zz}, blu dots) of the system (dots in the light yellow region). (b) Initial position of the selected nodes. In order to measure NE_{xx}, fifteen nodes (red dots) were selected on a vertical cross-section of the gel at approximately 30 μm from the pillar. These nodes were organized in a 5x3 matrix (i.e. 5 positions along the gel vertical dimension and 3 positions along the microchannel axis). In order to measure NE_{zz}, twenty-five nodes (cyan dots) were selected on a vertical cross-section of the gel normal to the microchannel axis, at approximately 27 μm from the periodic boundary. These nodes were organized in a 5x5 matrix (i.e. 5 positions along the gel vertical dimension and 5 positions along the pillar-to-pillar direction). (c) Final position of the selected nodes.

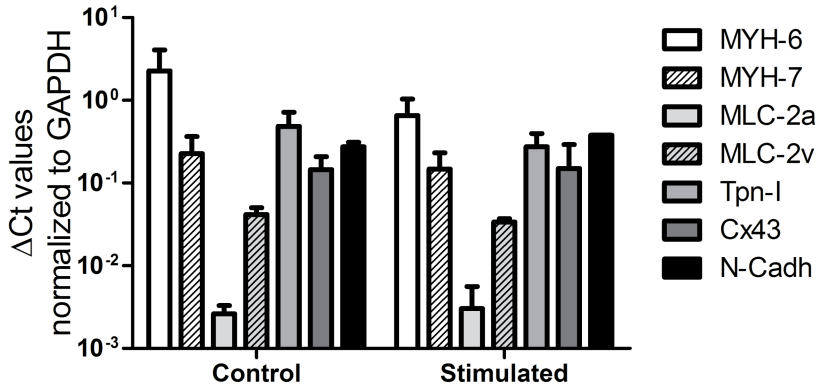

Fig. S6. Real-time RT-PCR analysis. Cardiac maturation was assessed in μECTs by quantifying the expression of main cardiac proteins as myosin heavy chain α and β (MYH-6 and MYH-7, respectively), myosin light chain atrial and ventricular (MLC-2a, corresponding to the gene MYL2, and MLC-2v, corresponding to gene MYL7), troponin I (Tpn-I), and gap and adherens junctions (Connexin-43 and N-Cadherin) in static (control) and stimulated conditions by quantitative real-time RT-PCR (N = 3). The graph shows relative expression compared with that of the housekeeping gene GAPDH.

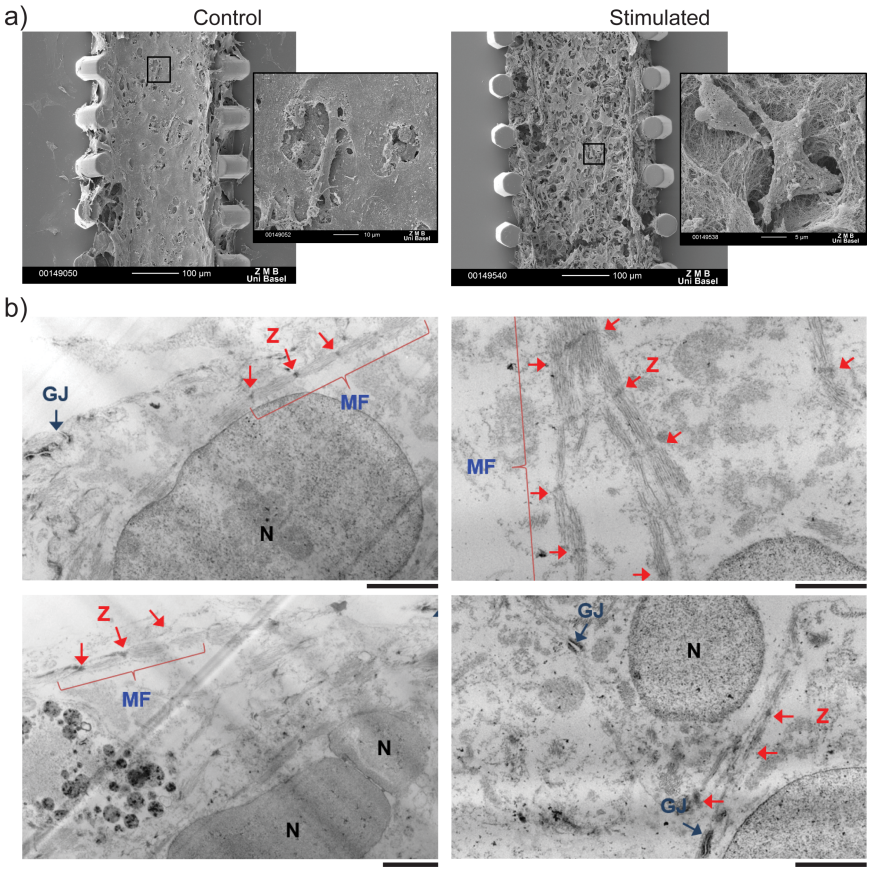

Fig. S7. Effect of uniaxial 3D cyclic mechanical strain on micro-cardiac constructs on extracellular matrix structure and organization and cell ultra-structure. (a) SEM images showing the remodeling of the fibrin gel after 6 days in culture within the microfluidic device in static (control) or stimulated conditions. Scale bar 100µm.

(b) Two representative TEM images of static cultured (left) and mechanical stimulated (right) micro-cardiac tissues after 6 days. Cardiomyocyte maturation and electrical coupling among cells (N indicates the cell nuclei) are shown by the presence of organized myofibrils (MF) with intercalated Z-disks (Z) and of gap junctions (GJ), respectively. Arrows indicate Z disks. Scale bar 2 µm.

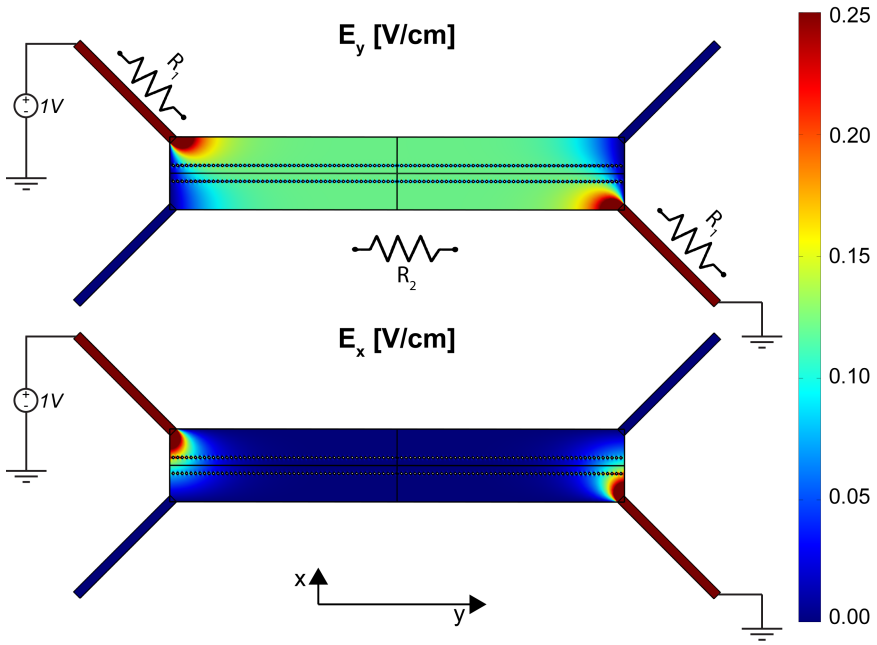

Fig. S8. Electric field distribution within the microdevice. A finite element numerical model was implemented to calculate the spatial distribution of electric field within the microfluidic device upon application of a 1V electric potential between two opposite wells (as indicated in the figure). Most of the electric potential drops within the cell culture channels, due to their reduced dimensions; on the contrary, the electric field is low, almost unidirectional along the channel (y direction) and rather constant throughout the cell culture chamber. Thanks to the linearity of the model, the electric field perceived by cells in culture can be estimated by scaling the computed value ($E_y \approx 0.12$ V/cm) according to the actual electric potential applied during stimulation. An electric equivalent circuit could be implemented, eliciting from geometrical considerations. The electric potential drop across the cells in culture was estimated through a voltage divider given by $R_2/(R_1+2R_2)$, as from the electric resistors sketched in the figure. The resulting factor, equal to 1/8.2 (≈ 0.122), was applied to correct the external electric field during experiments thus providing the actual electric potential perceived by cells.

Legends to Supplementary Movies

Movie S1.

Hydrogel pre-polymer injection procedure. The main video shows a lateral view of the injection process performed manually and acquired in real time. The high magnification inset evidences how the gel remains confined throughout the injection. Fibrin pre-polymer was colored with a blue dye to enhance the visualization.

Movie S2.

Evolution of gel nominal strains during device actuation. Evolution of gel nominal strains in the pillar-to-pillar direction (NE_{xx}) throughout the progressive loading of the PDMS membrane by a pressure increasing up to 0.5 atm.

Movie S3.

Uniaxial strain transferred to cardiac cells. The cyclic compression applied to the culture chamber results in a cyclic strain of the cell-laden fibrin gel. The video shows that the strain is highly uniaxial, in the direction perpendicular to the culture chamber main axis (in the top view). To better show how the load is transferred to individual cells, a low cell density was used to prepare the fibrin pre-polymer.

Movie S4.

Uniaxial strain transferred to micro-cardiac constructs. The cyclic compression applied to the culture chamber results in a cyclic strain of the cell-laden fibrin gel. The video shows that the strain is highly uniaxial, in the direction perpendicular to the culture chamber main axis (in the top view). In this video, the cell-laden fibrin gel was prepared with the desired target concentration of 1×10^5 cells/µl.

Movie S5.

Spontaneous beating of a control micro-cardiac construct. The maturation of micro-cardiac constructs was assessed by recording their spontaneous beating activity on a daily basis and throughout the entire culture period. Cell beating was generally observed starting from day 3 in both mechanical stimulated and control conditions. However, as shown in this representative video, the control micro-cardiac constructs exhibited poorly organized contractions and highly asynchronous events along the constructs.

Movie S6.

Spontaneous beating of a mechanically stimulated micro-cardiac construct. The maturation of micro-cardiac constructs was assessed by recording their spontaneous beating activity on a daily basis and throughout the entire culture period. Cell beating was generally observed starting from day 3 in both mechanical stimulated and control conditions. As shown in this representative video, the stimulated micro-cardiac constructs exhibited highly organized contractions, resulting in constructs beating synchronously in their entirety.

Movie S7.

Spontaneous beating of cardiac micro-constructs generated with iPSC derived CM. A cardiac micro-construct spontaneously beating. The construct was generated from human iPSC-derived cardiomyocytes cultured for 5 days under cyclic mechanical stimulation. The overview obtained with a motorized stage shows the synchronicity of the beating in all areas of the construct.